

Acoustic radiation force and torque on spheroidal particles in an ideal cylindrical chamber

José P. Leão-Neto,¹ Mauricio Hoyos,² Jean-Luc Aider,² and Glauber T. Silva^{3, a}

¹*Campus Arapiraca/Unidade de Ensino Penedo, Universidade Federal de Alagoas, Penedo, AL 57200-000, Brazil*

²*Laboratoire de Physique et Mécanique des Milieux Hétérogènes, UMR7636 CNRS, UMPC, ESPCI, 10 rue Vauquelin, 75005 Paris, France*

³*Physical Acoustics Group, Instituto de Física, Universidade Federal de Alagoas, Maceió, AL 57072-970, Brazil*

(Dated: 21 September 2020)

We theoretically investigate how the acoustic radiation force and torque arise on a small spheroidal particle immersed in a nonviscous fluid inside an ideal cylindrical chamber. The ideal chamber comprises a hard top and bottom (rigid boundary condition), and a soft or hard lateral wall. By assuming the particle is much smaller than the acoustic wavelength, we present analytical expressions of the radiation force and torque caused by an acoustic wave of arbitrary shape. Unlike previous results, these expressions are given relative to a fixed laboratory frame. Our model is showcased for analyzing the behavior of an elongated metallic microspheroid (with a 10 : 1 aspect ratio) in a half-wavelength acoustofluidic chamber with a few millimeters diameter. The results show the radiation torque aligns the microspheroid along the nodal plane, and the radiation force causes a translational motion with a speed of up to one body length per second. At last, we discuss the implications of this study to propelled nanorods by ultrasound.

©2020 Acoustical Society of America. [<https://doi.org/DOI number>]

[XYZ]

Pages: 1–11

I. INTRODUCTION

Techniques for particle manipulation in acoustofluidic chambers (acoustic resonators at millimeter-scale and smaller) have been extensively used in cell separation and sorting,¹ microparticle patterning,² and vesicle deformation.^{3,4} At the core of these methods is the radiation force of acoustic waves. This phenomenon is a stationary force caused by the linear-momentum flux change during the scattering of an incoming acoustic wave by a particle.^{5,6} Another related effect is the acoustic radiation torque caused by the angular-momentum flux change due to the presence of an anisotropic or absorptive particle.^{7–12}

Computing the radiation force and torque in acoustofluidic settings is essential to developing applications for cell analysis and analytical chemistry.¹³ On that matter, the forces and torques caused by a standing-wave field have been investigated considering spherical particles only.^{14–21} There is an increasing interest in studying the behavior of elongated particles in acoustofluidic resonators such as fibers,^{22,23} microrods,^{24,25} nanorods,^{26,27} *C. elegans*,²⁸ and *E. coli*.²⁹

Geometrically speaking, an elongated particle can be modeled as a prolate spheroid with a high aspect ratio. The analytical solution of the radiation force and

torque exerted on a prolate spheroid by a standing plane wave has been recently derived.^{30–33} In that sense, the effects of particle compressibility and density have been accounted for by using a method based on the Born approximation.^{34,35} Also, the acoustic spin-torque transfer to a spheroid has also been studied.³⁶ Another resort to compute acoustic forces and torques on complex-shaped particles rely on numerical methods.^{37–39} It is worth mentioning that the well-known *T*-matrix approach has also been applied to compute these fields.^{40,41}

In this article, we present a theoretical model to calculate the radiation force and torque on spheroidal particles in an ideal acoustic chamber filled with a nonviscous fluid. Our approach is based on the exact expressions of these fields to the dipole approximation as obtained in Ref. 42. We transform the radiation force and torque expressions to a fixed laboratory frame in which the particle dynamics can be analyzed. Thus, we focus our investigation on a chamber that produces a single levitation plane (half-wavelength trapping device) with radially symmetric modes. This appears to be more suitable for studying living matter²⁹ and developing techniques of cell culture.⁴³

We apply the developed model to study artificial microswimmers (micro/nanorods) propelled by ultrasound within a cylindrical chamber. The synthetic microswimmers have attracted attention due to their potential use for drug delivery⁴⁴ and activation inside living cells.⁴⁵ However, the propulsion mechanism of microswimmers

^agtomaz@fis.ufal.br

propelled by ultrasound is still a matter of debate. Nadal and Lauga⁴⁶ proposed an acoustic streaming model based on the asymmetry of a near-spherical particle that is vibrating at the wave frequency. Collins *et al.*⁴⁷ included density asymmetry to this model. However, a recent article questioned the validity of the acoustic streaming model for a vibrating near-sphere at low Reynolds number.⁴⁸ In our model, we consider an artificial microswimmer as a slender microspheroid. We predict the microswimmer is trapped in a levitation plane, not necessarily a nodal plane, due to the axial radiation force. When the levitation and nodal planes coincide, the radiation torque aligns the microspheroid perpendicularly to the chamber's principal axis. The radial radiation force causes an in-plane particle movement with a speed of about one body length per second (BL s^{-1}). This suggests the radiation force minimally contributes to the observed fast speeds of microswimmers, e.g., up to 70 BL s^{-1} .²⁶ Although our model does not explain microswimmers' propulsion mechanism, it presents some useful insights into the dynamics of these objects in a cylindrical chamber.

II. PHYSICAL MODEL

A. Acoustic equations

The interaction between an acoustic wave and a particle takes place inside a cylindrical chamber filled with a liquid of density ρ_0 , adiabatic speed of sound c_0 , and compressibility $\beta_0 = 1/\rho_0 c_0^2$. The chamber has radius R and height H . The acoustic excitation has angular frequency ω , with corresponding wavenumber $k = \omega/c_0 = 2\pi/\lambda$, where λ is the acoustic wavelength. We use the complex-phase representation to express the acoustic pressure and fluid velocity, $p(\mathbf{r}, t) = p(\mathbf{r})e^{-i\omega t}$ and $\mathbf{v}(\mathbf{r}, t) = \mathbf{v}(\mathbf{r})e^{-i\omega t}$, respectively. Here i is the imaginary unit, \mathbf{r} is position vector, and t is time.

The wave dynamics in a nonviscous fluid is described by the well-known acoustic equations

$$(\nabla^2 + k^2)p = 0, \quad (1a)$$

$$\mathbf{v} = \frac{\nabla p}{i\rho_0 c_0 k}. \quad (1b)$$

The term $e^{-i\omega t}$ is omitted for readability. The acoustic equations are complemented by boundary condition at the top, bottom, and walls of the cavity.

B. Prolate spheroidal particle

We assume the interacting particle with the acoustic wave is a prolate spheroid, which is generated by rotating an ellipse around its major axis. Let us define the particle frame of reference as a right-handed system $O_p(x_p, y_p, z_p)$ placed in the geometric center of the spheroid. The corresponding unit vectors of the system are \mathbf{e}_{x_p} , \mathbf{e}_{y_p} , and \mathbf{e}_{z_p} . The spheroid foci are at $(0, 0, \pm d/2)$, with r_1 and r_2 being the distance from the foci to a field point—see Fig. 1. The prolate spheroidal coordinates $(\xi_p, \eta_p, \varphi_p)$

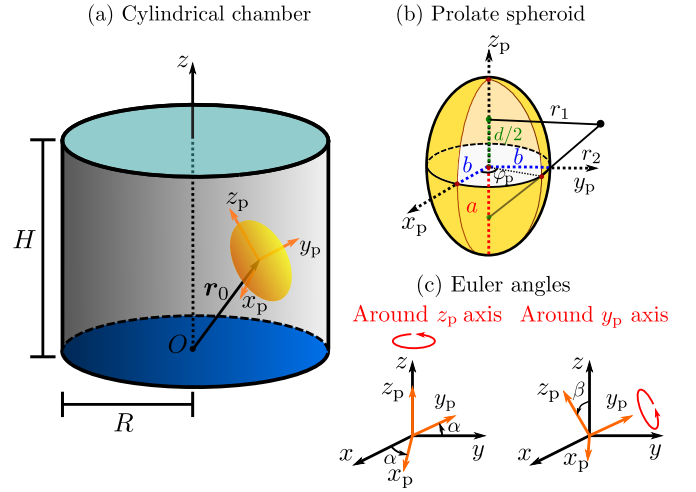


FIG. 1. (a) The cylindrical acoustic chamber with a (yellow) spheroid located at \mathbf{r}_0 regarding the laboratory frame O in the center of the chamber's bottom. (b) The prolate spheroid with major and minor semiaxis denoted by a and b , respectively. The interfocal distance is d . The quantities r_1 and r_2 are the distance from the foci to a field point. (c) The rotational transformations through the Euler angles α and β , which take the laboratory (x, y, z) to particle frame (x_p, y_p, z_p) .

are defined by

$$\xi_p = \frac{r_1 + r_2}{d}, \quad \xi_p \geq 1, \quad (2a)$$

$$\eta_p = \frac{r_1 - r_2}{d}, \quad -1 \leq \eta_p \leq 1, \quad (2b)$$

$$\varphi_p = \tan^{-1} \left(\frac{y_p}{x_p} \right), \quad 0 \leq \varphi_p < 2\pi, \quad (2c)$$

with the isosurface

$$\xi_p = \xi_0 = \frac{1}{\sqrt{1 - (b/a)^2}} \quad (3)$$

corresponding to the particle surface. Also, the particle major and minor axis are denoted by $2a$ and $2b$, respectively. While the interfocal distance and particle volume are given, respectively, by $d = 2\sqrt{a^2 - b^2}$ and $V_p = 4\pi ab^2/3$. The spheroid orientation in the particle frame coincides to the z_p axis, $\mathbf{d}_p = d\mathbf{e}_{z_p}$.

Note that a sphere of radius a is recovered by setting $d \rightarrow 0$, $\xi_0 \rightarrow \infty$, and $\xi_0 d/2 \rightarrow a$. Whereas, a slender spheroid corresponds to the limit $\xi_0 \rightarrow 1$ with a constant d . In contrast, a slender spheroid results from $\xi_0 \sim 1$.

C. Particle versus laboratory frame of reference

It is convenient to describe the wave-particle interaction in an inertial frame $O(x, y, z)$ referred to as the laboratory system. In Fig. 1(a), we see the origin of the laboratory frame is positioned at the center of the chamber's bottom. And the particle position is denoted by

vector \mathbf{r}_0 . Since the spheroidal particle is invariant under rotations around its major axis, we need only two Euler angles (α, β) to transform one frame to the other—see Fig. 1(c). The transformation from the laboratory to particle frame is constructed as follows. A positive rotation of an azimuthal angle α around the z_p axis is followed by a rotation of a polar angle β about the new y_p axis. By a positive rotation we mean a counterclockwise rotation as seen from the top of the rotation axis. The particle orientation in the laboratory frame is then given by

$$\begin{aligned} \mathbf{d} &= \mathbf{R}(\alpha, \beta) \mathbf{d}_p \\ &= d (\cos \alpha \sin \beta \mathbf{e}_x + \sin \alpha \sin \beta \mathbf{e}_y + \cos \beta \mathbf{e}_z), \end{aligned} \quad (4a)$$

$$\mathbf{R}(\alpha, \beta) = \begin{pmatrix} \cos \alpha \cos \beta & -\sin \alpha & \cos \alpha \sin \beta \\ \sin \alpha \cos \beta & \cos \alpha & \sin \alpha \sin \beta \\ -\sin \beta & 0 & \cos \beta \end{pmatrix}, \quad (4b)$$

with $0 \leq \alpha < 2\pi$ and $0 \leq \beta \leq \pi$. It is worth noticing the gradient operator is transformed as,

$$\nabla = \mathbf{R}(\alpha, \beta) \nabla_p |_{\mathbf{r}_p=\mathbf{r}}, \quad \nabla_p = \mathbf{R}^{-1}(\alpha, \beta) \nabla |_{\mathbf{r}=\mathbf{r}_p}, \quad (5)$$

where \mathbf{R}^{-1} represents the transformation from the laboratory to the particle frame.

D. Acoustic modes in a cylindrical cavity

The acoustic modes allowed inside the cavity are the solutions of Eq. (1a) in cylindrical coordinates $\mathbf{r}(\varrho, \varphi, z)$. Accordingly, the pressure inside the chamber is¹⁴

$$p(\mathbf{r}) = p_0 J_n(k_\varrho \varrho) \cos(n\varphi + \varphi_0) \cos k_z z, \quad (6)$$

where p_0 is the pressure magnitude, J_n is the n th-order Bessel function, k_ϱ and k_z are the radial and axial wave numbers, and φ_0 is an arbitrary constant.

The radial, angular, and axial modes are determined from boundary conditions. We consider hard boundaries at the bottom ($z = 0$) and top ($z = H$) of the chamber. While for the lateral wall ($\varrho = R$), a hard or soft boundary is assumed. Accordingly, the fluid velocity and pressure satisfy

$$v_z(\varrho, \varphi, 0) = 0, \quad v_z(\varrho, \varphi, H) = 0, \quad (7a)$$

$$v_\varrho(R, \varphi, z) = 0 \text{ (hard)}, \quad p(R, \varphi, z) = 0, \text{ (soft)}. \quad (7b)$$

Since we do not have a tangential boundary condition, the phase φ_0 can be arbitrarily set to zero. The conditions in (7) imply

$$\sin(k_z H) = 0, \quad (8a)$$

$$J'_n(k_\varrho R) = 0 \text{ (hard)}, \quad J_n(k_\varrho R) = 0 \text{ (soft)}. \quad (8b)$$

Here the primed symbol denotes ordinary differentiation. The solutions of these equations yield the axial and radial dispersion relations,

$$k_z = k_l = \frac{l\pi}{H}, \quad (9a)$$

$$k_\varrho = k_{nm} = \frac{j_{nm}}{R} \text{ (soft)}, \quad \frac{j'_{nm}}{R} \text{ (hard)}, \quad (9b)$$

TABLE I. The first five zeros of the zeroth- and first-order Bessel functions.⁴⁹

m	1	2	3	4	5
$j_{0,m}$	2.4048	5.5201	8.6537	11.7915	14.9309
$j_{1,m}$	3.8317	7.0156	10.1735	13.3237	16.4706

with $n = 0, 1, 2, \dots$; $l, m = 1, 2, 3, \dots$. The m th positive zero of the n th Bessel function and its derivative are j_{nm} and j'_{nm} , respectively. The total wave number is given by

$$k = \sqrt{k_l^2 + k_{nm}^2}. \quad (10)$$

We see the angular frequency $\omega = kc_0$ is quantized.

In what follows, we analyze radially-symmetric acoustic modes that forms a half-wavelength acoustofluidic chamber, $(nml) = (0m1)$. Hence, the wave numbers turn to

$$k_1 = \frac{\pi}{H}, \quad k_{0m} = \frac{j_{0,m}}{R} \text{ (soft)}, \quad k_{0m} = \frac{j'_{1,m}}{R} \text{ (hard)}. \quad (11)$$

We have used the relation between the zeros of the Bessel functions $j'_{0,m} = j_{1,m}$. In Table I, we list the first five zeros of the zeroth- and first-order Bessel functions for reference.

We now express the pressure of the radially-symmetric modes,

$$p_{0m1} = p_0 J_0(k_{0m} \varrho) \cos(k_1 z). \quad (12)$$

Substituting this equation into Eq. (1b) yields the radial and axial components of the fluid velocity

$$v_\varrho = \frac{iv_0 k_{0m}}{k} J_1(k_{0m} \varrho) \cos(k_1 z), \quad (13a)$$

$$v_z = \frac{iv_0 k_1}{k} J_0(k_{0m} \varrho) \sin(k_1 z), \quad (13b)$$

where $v_0 = p_0/\rho_0 c_0$ is the peak velocity. Note we have used $J'_0(x) = -J_1(x)$.

E. Scale analysis

We assume that the particle is a subwavelength spheroid much smaller than the wavelength, which corresponds to the so-called Rayleigh scattering limit. The particle smallness is quantified through the size factor

$$ka = \frac{2\pi a}{\lambda} \ll 1. \quad (14)$$

Clearly, the minor semiaxis b also satisfies this condition. We also restrict our analysis to particles much smaller to the chamber, $a, b \ll H, R$.

Another effect that may appear in an acoustofluidic chamber is the acoustic streaming, which appear near boundaries. Acoustic streaming close to the chamber walls produces causes a drag force on the particle, while near the particle surface, it can alter the radiation

force^{50–52} and produce a viscous torque.⁵³ As a diffusive process, streaming has a characteristic length known as the viscous boundary layer, $\delta = (2\mu_0/\rho_0\omega)^{1/2}$, with μ_0 being the dynamic viscosity of the fluid. To avoid streaming effects, we should consider particles much larger than this parameter, $\delta \ll a, b$. For example, an acoustic wave of a frequency greater than 1 MHz (a typical lower limit for acoustofluidic devices) in water generates a viscous boundary layer $\delta < 0.84 \mu\text{m}$.

III. WAVE-PARTICLE NONLINEAR INTERACTION

A. Acoustic radiation force

The radiation force imparted on a subwavelength spheroidal particle by a stationary wave is expressed by⁴²

$$\begin{aligned} \mathbf{F}_p^{\text{rad}}(\mathbf{0}) &= -\nabla_p U_p(\mathbf{0}), \\ U_p &= \pi a^3 \\ &\left[\frac{\beta_0 f_{00}}{3} |p|^2 - \frac{\rho_0}{2} \left(\frac{f_{11}}{2} (|v_{x_p}|^2 + |v_{y_p}|^2) + f_{10} |v_{z_p}|^2 \right) \right], \end{aligned} \quad (15a)$$

$$(15b)$$

where $E_0 = \beta_0 p_0^2/2$ is the characteristic energy density, and $\mathbf{v}_p = (v_{x_p}, v_{y_p}, v_{z_p})$ is the fluid velocity in the particle frame. Considering a rigid particle, the scattering amplitudes of the monopole f_{00} , axial f_{10} and transverse f_{11} dipole modes are given by⁴²

$$f_{00} = 1 - \xi_0^{-2}, \quad (16a)$$

$$f_{10} = \frac{2}{3\xi_0^3} \left[\frac{\xi_0}{\xi_0^2 - 1} - \ln \left(\frac{\xi_0 + 1}{\sqrt{\xi_0^2 - 1}} \right) \right]^{-1}, \quad (16b)$$

$$f_{11} = \frac{8}{3\xi_0^3} \left[\frac{2 - \xi_0^2}{\xi_0(\xi_0^2 - 1)} + \ln \left(\frac{\xi_0 + 1}{\sqrt{\xi_0^2 - 1}} \right) \right]^{-1}. \quad (16c)$$

These factors depend on the particle aspect ratio a/b through the parameter ξ_0 introduced in Eq. (3). After

inspecting (16), we find the following inequalities

$$0 < f_{00} < f_{11} < 2, \quad 0 < 2f_{10} < f_{11} < 2. \quad (17)$$

As the particle geometry becomes spherical, the dipole factors turn into $f_{11} \rightarrow 2f_{10}$. Whereas, slender particles scatter much less acoustic waves,

$$f_{00}, f_{10}, f_{11} \rightarrow 0 \text{ as } \xi_0 \rightarrow 1. \quad (18)$$

It is more convenient to analyze the radiation force on the particle in the laboratory frame. To this end, we have to express the acoustic fields of Eq. (15b) in the laboratory frame. By inserting the velocity components of (A2) into (15b), we obtain the radiation force potential in this frame as

$$\begin{aligned} U &= \pi a^3 \left[\frac{\beta_0 f_{00}}{3} |p|^2 - \frac{\rho_0}{2} \left(f_{10} |(v_x \cos \alpha + v_y \sin \alpha) \sin \beta \right. \right. \\ &\quad \left. \left. + v_z \cos \beta|^2 + \frac{1}{2} f_{11} [|v_x \sin \alpha - v_y \cos \alpha|^2 \right. \right. \\ &\quad \left. \left. + |v_x \cos \alpha \cos \beta + v_y \sin \alpha \cos \beta - v_z \sin \beta|^2] \right) \right]. \end{aligned} \quad (19)$$

To find the potential in cylindrical coordinates, we use $v_x = v_\varrho \cos \varphi$, $v_y = v_\varrho \sin \varphi$. Thus, we have

$$\begin{aligned} U &= \pi a^3 \left[\frac{\beta_0 f_{00}}{3} |p|^2 - \frac{\rho_0}{2} \left(f_{10} |v_\varrho \sin \beta \cos(\alpha - \varphi) \right. \right. \\ &\quad \left. \left. + v_z \cos \beta|^2 + \frac{f_{11}}{2} [|v_\varrho \cos \beta \cos(\alpha - \varphi) \right. \right. \\ &\quad \left. \left. - v_z \sin \beta|^2 + |v_\varrho|^2 \sin^2(\alpha - \varphi)] \right) \right]. \end{aligned} \quad (20)$$

Now, substituting the pressure and fluid velocity components given in Eqs. (12) and (13) into Eq. (20), we obtain the potential of the radially-symmetric acoustic modes,

$$\begin{aligned} U_{0m1} &= U_0 \left\{ \frac{2f_{00}}{3} \cos^2(k_1 z) J_0^2(k_{0m} \varrho) - f_{10} \left[\frac{k_1}{k} \sin(k_1 z) J_0(k_{0m} \varrho) \cos \beta + \frac{k_{0m}}{k} \cos(k_1 z) J_1(k_{0m} \varrho) \cos(\alpha - \varphi) \sin \beta \right]^2 \right. \\ &\quad \left. - \frac{f_{11}}{2} \left[\left(\frac{k_1}{k} \sin(k_1 z) J_0(k_{0m} \varrho) \sin \beta - \frac{k_{0m}}{k} \cos(k_1 z) J_1(k_{0m} \varrho) \cos \beta \cos(\alpha - \varphi) \right)^2 + \left(\frac{k_{0m}}{k} \right)^2 \cos^2(k_1 z) J_1^2(k_{0m} \varrho) \right. \right. \\ &\quad \left. \left. \sin^2(\alpha - \varphi) \right] \right\}, \end{aligned} \quad (21)$$

where $U_0 = \pi a^3 E_0$ is the peak potential. For simplicity, we drop the sub-index 0 of the particle position in cylindrical coordinates, $\mathbf{r}_0 = (\varrho, \varphi, z)$.

By fixing the height and diameter of the chamber, the normalized potential $\tilde{U}_{0m1} = U_{0m1}/U_0$ depends only

on the particle aspect ratio a/b through the scattering factors f_{00} , f_{10} , and f_{11} . The potential also depends on the orientation angles α and β , and to the azimuthal angle φ , albeit the $(0m1)$ acoustic mode in Eq. (12) has circular symmetry. As the particle becomes spherical

($f_{11} \rightarrow 2f_{10}$), Eq. (21) reduces to the radiation potential of a spherical particle as given in Ref. 14, Eq. 1, with $m = 0$ in the reference's notation.

Having discussed how the potential function is obtained, we are able to derive the radiation force in the laboratory frame. From Eqs. (4b) and (5), we find this force as minus the gradient of the potential given in Eq. (21),

$$\begin{aligned} \mathbf{F}^{\text{rad}} &= \mathbf{R}^{-1}(\alpha, \beta) \mathbf{F}_p^{\text{rad}} = -\mathbf{R}^{-1}(\alpha, \beta) \nabla_p U_p(\mathbf{0}) \\ &= -\nabla U(\mathbf{r}_0). \end{aligned} \quad (22)$$

Thus far, we derived the exact solution of the radiation force problem for the particle placed anywhere inside the chamber. We can distill this solution for two particular cases, namely, along the chamber's axis of symmetry and at the nodal plane. For the first case, the potential and radiation force are derived using Eqs. (12) and (13) into Eq. (21) and setting $\varrho = 0$. The obtained result is used in Eq. (22). Accordingly, we arrive at

$$U_{0m1} = \frac{U_0}{6} \left[4f_{00} \cos^2(k_1 z) - 3 \left(\frac{k_1}{k} \right)^2 \sin^2(k_1 z) \right. \\ \left. (2f_{10} \cos^2 \beta + f_{11} \sin^2 \beta) \right], \quad (23a)$$

$$F_z^{\text{rad}} = F_{0,z} \Phi_a \sin(2k_1 z), \quad (23b)$$

$$\Phi_a = \frac{2f_{00}}{3} + \left(\frac{k_1}{k} \right)^2 \left(f_{10} \cos^2 \beta + \frac{f_{11}}{2} \sin^2 \beta \right), \quad (23c)$$

with $F_{0,z} = k_1 U_0$ being the axial force magnitude. The function Φ_a is the axial acoustophoretic factor which depends on the scattering modes and orientation angle β . Referring to the inequalities in (17), we conclude that $\Phi_a > 0$. When effects of gravity can be neglected, the rigid spheroidal particle is trapped in the pressure node, $z_{\text{eq}} = H/2$. Note the maximum axial force corresponds to $F_{z,\text{max}} = F_{0,z} \Phi_a$ at $z = H/4, 3H/4$.

To obtain the radiation force potential in the nodal plane $z_{\text{eq}} = H/2$, we see from (13) the pressure and the radial component of the fluid velocity vanish, $p_{0m1} = 0$ and $v_\varrho = 0$. From Eq. (20), we find

$$U_{0m1} = -\pi a^3 \Phi_r(\beta) \frac{\rho_0 |v_z|^2}{2}, \quad (24a)$$

$$\Phi_r(\beta) = f_{10} \cos^2 \beta + \frac{f_{11}}{2} \sin^2 \beta. \quad (24b)$$

The radiation force potential is a function of the axial component of the kinetic energy density. Besides, the acoustophoretic factor Φ_r does not depend on the monopole scattering mode f_{00} . This happens because the pressure vanishes at the nodal plane and so does the monopole term in Eq. (21). After substituting Eq. (13b) into Eq. (24a) and replacing the result into Eq. (22), we

obtain the potential and radial radiation force as

$$U_{0m1} = - \left(\frac{k_1}{k} \right)^2 U_0 \Phi_r(\beta) J_0^2(k_{0m} \varrho), \quad (25a)$$

$$F_\varrho^{\text{rad}} = -F_{0,\varrho} \Phi_r(\beta) J_0(k_{0m} \varrho) J_1(k_{0m} \varrho), \quad (25b)$$

$$F_{0,\varrho} = 2 \left(\frac{k_1}{k} \right)^2 k_{0m} U_0, \quad (25c)$$

with $F_{0,\varrho}$ being the force magnitude. The radial acoustic traps correspond to the minima of the potential function, while the largest force occurs at $k_{0m} \varrho = 1.081$, with corresponding magnitude of $F_{\varrho,\text{max}}^{\text{rad}} = 0.338 F_{0,\varrho} \Phi_r$. For a rigid particle, the radial acoustophoretic factor is positive and the potential minima are obtained by solving the equation $J_0^2(k_{0m} \varrho) = 0$. This corresponds to find the zeros of the first-order Bessel function. Hence, the position of the i th radial trapping point is at

$$\varrho_{i,m} = \frac{j_{1,i-1}}{j_{0,m}} R \text{ (soft)}, \quad \frac{j_{1,i-1}}{j_{1,m}} R \text{ (hard)}, \quad m = 1, 2, \dots \quad (26)$$

Here we consider $j_{1,0} = 0$. The primary trap corresponds to $\varrho_{1,m} = 0$ regardless the lateral boundary condition, e.g., soft or hard wall. To determine the second trap position, we refer to Table I, $\varrho_{2,1} = 0.63R$ (soft wall) and $\varrho_{2,1} = R$ (hard wall). We see soft walled chambers are able to produce only a middle trap. Whereas, the second trap of a hard walled chamber is located at the lateral wall.

B. Acoustic radiation torque

The acoustic radiation torque exerted on the spheroidal particle by the acoustic mode described in Eq. (12), is given in the particle frame by⁴²

$$\boldsymbol{\tau}_p^{\text{rad}} = -\pi a^3 \chi (\mathbf{e}_{z_p} \times \mathbf{P}_p \cdot \mathbf{e}_{z_p})_{\mathbf{r}_p=\mathbf{0}}, \quad (27a)$$

$$\mathbf{P}_p = \frac{\rho_0}{2} \text{Re}[\mathbf{v}_p \mathbf{v}_p^*] = \frac{\rho_0}{2} \text{Re}[v_i v_j^* \mathbf{e}_i \mathbf{e}_j], \quad i, j = x_p, y_p, z_p, \quad (27b)$$

where $\chi = f_{11} - 2f_{10} > 0$ is the gyroacoustic factor and \mathbf{P}_p is the time-average of the linear momentum flux (a second-rank tensor) relative to the particle frame. We express the projection of the linear momentum flux onto the axial direction as $\mathbf{P}_p \cdot \mathbf{e}_{z_p} = (\rho_0/2) \text{Re}[v_{z_p}^* \mathbf{v}_p]$. Carrying on the calculations, we arrive at

$$\boldsymbol{\tau}_p^{\text{rad}} = \frac{\pi a^3}{2} \chi \rho_0 \text{Re} \left[v_{y_p} v_{z_p}^* \mathbf{e}_{x_p} - v_{x_p} v_{z_p}^* \mathbf{e}_{y_p} \right]. \quad (28)$$

To find the radiation torque in the laboratory frame, we apply the rotation matrix \mathbf{R} into Eq. (28),

$$\begin{aligned} \boldsymbol{\tau}^{\text{rad}} &= \mathbf{R}(\alpha, \beta) \boldsymbol{\tau}_p^{\text{rad}} \\ &= \frac{\pi a^3}{2} \chi \rho_0 \text{Re} \left[(v_{y_p} v_{z_p}^* \cos \alpha \cos \beta + v_{x_p} v_{z_p}^* \sin \alpha) \mathbf{e}_x \right. \\ &\quad \left. + (v_{y_p} v_{z_p}^* \sin \alpha \cos \beta - v_{x_p} v_{z_p}^* \cos \alpha) \mathbf{e}_y \right. \\ &\quad \left. - v_{y_p} v_{z_p}^* \sin \beta \mathbf{e}_z \right]. \end{aligned} \quad (29)$$

Substituting the fluid velocity components given in Eq. (13) into Eq. (A3) and replacing the result into Eq. (29), we obtain

$$\tau_x = -\frac{\pi a^3 \chi E_0}{2} \left[\left(\frac{k_1}{k} \right)^2 \sin 2\beta \sin \alpha \sin^2(k_1 z) J_0^2(k_{0m} \varrho) + \frac{k_1 k_{0m}}{k^2} \sin(2k_1 z) J_0(k_{0m} \varrho) J_1(k_{0m} \varrho) \right. \\ \left. [\sin^2 \beta \sin \alpha \cos(\alpha - \varphi) + \cos^2 \beta \sin \varphi] - \left(\frac{k_{0m}}{k} \right)^2 \sin 2\beta \cos^2(k_1 z) \sin \varphi J_1^2(k_{0m} \varrho) \cos(\alpha - \varphi) \right], \quad (30a)$$

$$\tau_y = \frac{\pi a^3 \chi E_0}{2} \left[\left(\frac{k_1}{k} \right)^2 \sin 2\beta \cos \alpha \sin^2(k_1 z) J_0^2(k_{0m} \varrho) + \frac{k_1 k_{0m}}{k^2} \sin(2k_1 z) J_0(k_{0m} \varrho) J_1(k_{0m} \varrho) \right. \\ \left. [\sin^2 \beta \cos \alpha \cos(\alpha - \varphi) - \cos^2 \beta \cos \varphi] - \left(\frac{k_{0m}}{k} \right)^2 \sin(2\beta) \cos^2(k_1 z) J_1^2(k_{0m} \varrho) \cos(\alpha - \varphi) \cos \varphi \right], \quad (30b)$$

$$\tau_z = \frac{\pi a^3 \chi E_0}{2} \left[\frac{k_1 k_{0m}}{2k^2} \sin 2\beta \sin(\alpha - \varphi) \sin(2k_1 z) J_0(k_{0m} \varrho) J_1(k_{0m} \varrho) + \left(\frac{k_{0m}}{k} \right)^2 \sin^2 \beta \cos^2(k_1 z) \sin[2(\alpha - \varphi)] \right. \\ \left. J_1^2(k_{0m} \varrho) \right]. \quad (30c)$$

When the particle is trapped at $z_{\text{eq}} = H/2$, we see from (13) that the radial component of the fluid velocity vanishes $v_\varrho = 0$. Hence, referring to Eqs. (A3) and (29), the radiation torque reduces to

$$\boldsymbol{\tau}^{\text{rad}} = \pi a^3 \chi \sin 2\beta \frac{\rho_0 |v_z|^2}{4} \mathbf{e}_\alpha. \quad (31)$$

The unit vector $\mathbf{e}_\alpha = \cos \alpha \mathbf{e}_y - \sin \alpha \mathbf{e}_x$ lies along the minor semiaxis pointing to the counterclockwise direction in the xy plane. The radiation torque is proportional to the axial component of the kinetic energy density averaged in time $\rho_0 |v_z|^2/4$. It also depends on the orientation factor $\sin 2\beta$. The particle is set to rotate around the minor axis, since $\mathbf{e}_\alpha \cdot \mathbf{e}_z = 0$. Now we replace v_z in Eq. (31) by Eq. (13b) to encounter

$$\boldsymbol{\tau}^{\text{rad}}(\beta) = \tau_0 \chi J_0^2(k_{0m} \varrho) \sin 2\beta \mathbf{e}_\alpha, \quad (32)$$

where $\tau_0 = \pi a^3 E_0 k_1^2 / 2k^2$ is the characteristic torque. The maximum torque $\tau_{\text{max}}^{\text{rad}} = \tau_0 \chi$, which occurs at $\beta = \pi/4$ and $\varrho = 0$. The equilibrium angular position corresponds to $\beta = \pi/2$.

C. Effects of gravity

An actual particle of density ρ_p is subjected to effects of gravity, which changes its axial equilibrium position. The new position can be determined from the force equilibrium equation $F^{\text{rad}}(0, z_{\text{eq}}) - (\rho_p - \rho_0) V_p g = 0$, with g being the gravity acceleration. Thus from Eq. (23b), the axial equilibrium position is

$$z_{\text{eq}} = \frac{H}{2} - \frac{H}{2\pi} \arcsin \left[\frac{4(\rho_p - \rho_0)gH}{3\pi\Phi_a E_0} \left(\frac{b}{a} \right)^2 \right]. \quad (33)$$

To bring the particle close to the nodal plane, we need to increase the acoustic energy density. From Eq. (33), we see the energy density needed to keep the particle in equilibrium is

$$E_0 = \frac{4(\rho_p - \rho_0)gH}{3\pi\Phi_a \sin(2\pi z_{\text{eq}}/H)} \left(\frac{b}{a} \right)^2. \quad (34)$$

We see that slender particles with $a \gg b$ require less energy to be axially trapped.

D. Translational and angular velocity of the particle

Here we obtain the stationary translational and angular velocity achieved by the particle at the nodal plane $z_{\text{eq}} = H/2$. This analysis is restricted to particles at microscale in an aqueous solution.

To determine the translational velocity, we assume the particle is at $(\varrho, \varphi, H/2)$ and aligned to the radial direction, $\beta = \pi/2$ and $\alpha = \varphi$. Hence the velocity is denoted by $\dot{\varrho}$, with dot notation meaning time derivative. As the particle moves, a drag force counteracts the radiation force,⁵⁴

$$\mathbf{F}^{\text{drag}} = -8\pi a \mu_0 g_f \dot{\varrho} \mathbf{e}_\varrho, \quad (35a)$$

$$g_f = \frac{1}{\xi_0 [(\xi_0^2 + 1) \operatorname{arccoth} \xi_0 - \xi_0]}. \quad (35b)$$

The geometric factor g_f becomes 3/4 for a spherical particle ($\xi_0 \rightarrow \infty$), which leads to the well-known Stoke's law, $F_{\text{sphere}}^{\text{drag}} = -6\pi \mu_0 a \dot{\varrho}$.

Using Eq. (25b), we find the equation of motion of a particle moving along its major axis as

$$\ddot{\varrho} + \frac{8\pi a \mu_0 g_f}{M} \dot{\varrho} = -\frac{F_{0,\varrho} \Phi_r}{M} J_0(k_{0m} \varrho) J_1(k_{0m} \varrho). \quad (36)$$

TABLE II. The physical and geometric parameters of the microswimmer in a submillimeter cylindrical chamber at room temperature and pressure.

Parameter	Value
Microspheroid (Au)	
Major semiaxis (a)	10 μm
Minor semiaxis (b)	1 μm
Aspect ratio (a/b)	10:1
Radial parameter (ξ_0)	1.0050
Volume (V_p)	41.9 μm^3
Density (ρ_p)	19 300 kg m^{-3}
Moment of inertia (I)	16.3 $\text{ng } \mu\text{m}^2$
Monopole mode (f_{00})	0.01
Axial dipole mode (f_{10})	0.0068
Transverse dipole mode (f_{11})	0.0261
Water	
Density (ρ_0)	1000 kg m^{-3}
Speed of sound (c_0)	1492 m s^{-1}
Cylindrical chamber²⁶	
Height (H)	180 μm
Radius (R)	2.5 mm
Levitation plane (z_{eq})	76.5 μm
Energy density (E_0)	15.3 J m^{-3}

TABLE III. The theoretical predictions of the microspheroid at the nodal plane considering the parameters of Table II.

Feature	Acoustic modes			
	Soft		Hard	
	(011)	(021)	(011)	(021)
Frequency [MHz]	4.150	4.177	4.160	4.197
Radial force, $F_{\rho, \text{max}}^{\text{rad}}$ [pN]	0.407	0.921	0.645	1.160
Translational velocity, $\dot{\varrho}$ [$\mu\text{m s}^{-1}$]	8.185	18.55	12.98	23.35
Trap time, t_ϱ [s]	43.05	8.277	17.04	5.174
Radiation torque, $\tau_{\text{max}}^{\text{rad}}$ [nN μm]	0.299	0.296	0.298	0.293
Angular velocity, $\dot{\beta}$ [rad s^{-1}]	23.62	23.02	23.40	22.58
Reorientation time, t_β [ms]	31.44	32.26	31.73	32.89

where M is the particle's mass. Considering a micrometer-sized particle in water, we see the viscous contribution overcomes inertia by far. So the inertial term in Eq. (36) can be neglected. The equation of motion then becomes

$$\dot{\varrho} = - \left(\frac{k_1}{k} \right)^2 \frac{k_{0m} a^2 \Phi_r E_0}{4g_t \mu_0} J_0(k_{0m}\varrho) J_1(k_{0m}\varrho). \quad (37)$$

We conclude the translational speed increases with the particle length squared. We find the solution of Eq. (37)

for a particle in the vicinity of $\varrho = 0$ with the initial position at $\varrho(0) = \varrho_0$,

$$\varrho(t) = \varrho_0 e^{-t/t_\varrho}, \quad (38a)$$

$$t_\varrho = \left(\frac{2k}{k_1 k_{0m} a} \right)^2 \frac{g_t \mu_0}{\Phi_r E_0}. \quad (38b)$$

Importantly, the characteristic trapping time t_ϱ is of the order of seconds.

Turning now to the angular velocity induced by the radiation torque of Eq. (32) on a particle at $(\varrho, \varphi, H/2)$. As the radiation torque depends only on the orientation angle β , the angular velocity corresponds to the rate change of the orientation, $\dot{\beta}$. Moreover, a drag torque arises on the particle,³³

$$\boldsymbol{\tau}^{\text{drag}} = -8\pi a^3 \mu_0 g_t \dot{\beta} \mathbf{e}_\alpha, \quad (39a)$$

$$g_t = \frac{4}{3\xi_0^3} \frac{1 - 2\xi_0^2}{2\xi_0 - (1 + \xi_0^2) \ln \left(\frac{\xi_0 + 1}{\xi_0 - 1} \right)}. \quad (39b)$$

The well-known result of the drag torque for a sphere, $\tau^{\text{drag}} = -8\pi a^3 \mu_0 \dot{\beta}$, is obtained by setting $\xi_0 \rightarrow \infty$.

The rotational particle dynamics is described by the differential equation

$$\ddot{\beta} + \frac{8\pi a^3 \mu_0 g_t}{I} \dot{\beta} = \frac{\tau_0 \chi J_0^2(k_{0m}\varrho)}{I} \sin 2\beta, \quad (40)$$

with $I = M(a^2 + b^2)/5$ being the particle moment of inertia relative to the minor axis. Again the viscous effects overcome inertia. So the rotational equation of motion becomes

$$\dot{\beta} = \frac{\tau_0 \chi J_0^2(k_{0m}\varrho) \sin 2\beta}{8\pi a^3 \mu_0 g_t}, \quad (41)$$

which can be solved by the method of separation of variables. Let β_0 be the initial particle orientation. Using the expression $\int \sin^{-1} 2\beta \, d\beta = \ln(\tan \beta)/2$, we find

$$\beta(t) = \text{arccot} \left[\exp \left(-\frac{t}{t_\beta J_0^2(k_{0m}\varrho)} \right) \cot \beta_0 \right], \quad (42a)$$

$$t_\beta = \left(\frac{4k}{k_1} \right)^2 \frac{g_t \mu_0}{\chi E_0}. \quad (42b)$$

The orientation angle asymptotically approaches $\beta = \pi/2$ (aligned with the nodal plane) as $t \rightarrow \infty$. Slender particles $\chi \rightarrow 0$ need more time to reach equilibrium, as well as particles far from the center. The characteristic reorientation time t_β is of the order of milliseconds.

The rotational-to-translational characteristic time ratio is about

$$\frac{t_\beta}{t_\varrho} \sim (k_{0m} a)^2. \quad (43)$$

This ratio is about 10^{-3} for typical acoustofluidic settings.

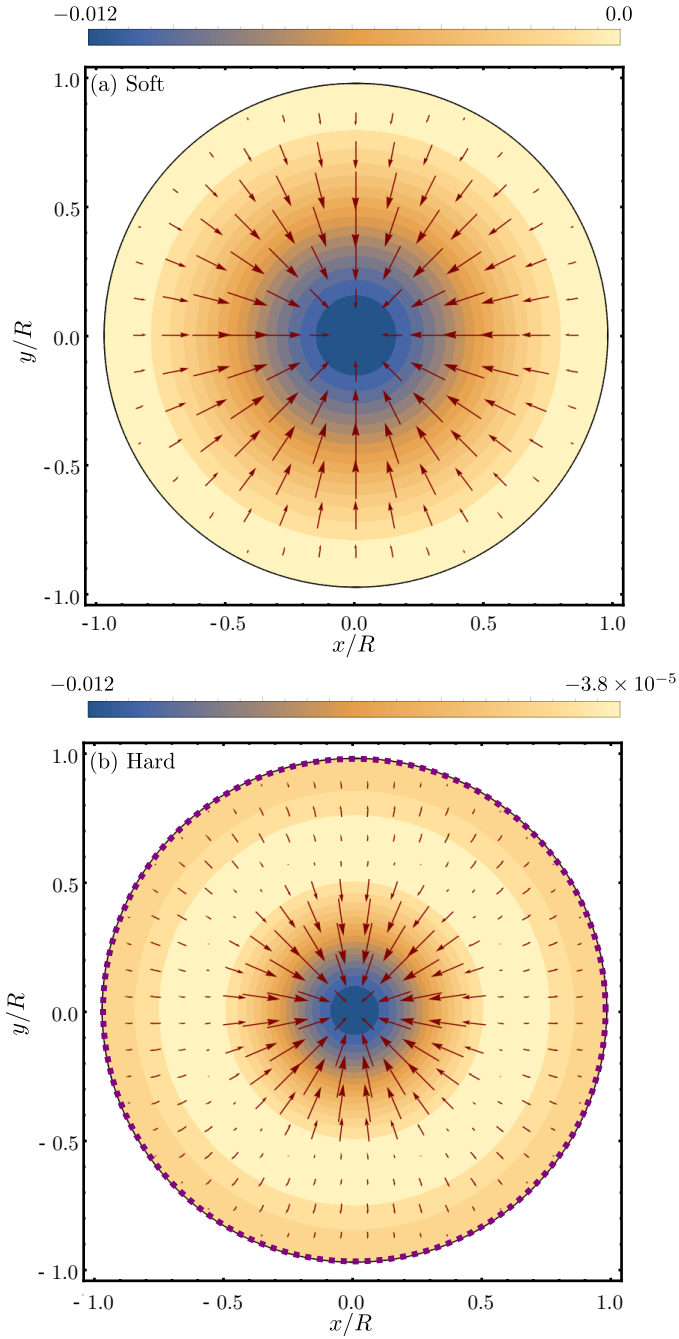


FIG. 2. The radiation force fields (red arrows) of the micro-spheroid aligned to the x axis. The force is generated by the (011) acoustic mode with (a) soft and (b) hard lateral walls. The background contours illustrate the potential function U_{011} , given by Eq. (21), normalized to $U_0 = 48.07$ fJ. The force fields are evaluated in the laboratory frame at the axial position $z_{\text{eq}} = 0.85H/2$. The physical parameters used here are listed in Table II. The bluish regions correspond to the middle trap, while the dotted-purple circle in panel (b) is the annular trap.

IV. CASE STUDY: AU MICRORODS

Now, we use the theory to analyze the radiation force and torque fields in a acoustofluidic chamber wherein the particles are trapped as described in Ref. 26. In this reference, the chamber operates at nearly 4 MHz, and the particles are metallic (Au) nanorods with length of few micrometers and hundreds of nanometers wide. These objects can be geometrically modeled as microspheroids with a slender shape. As the particle width is of the order of the viscous boundary layer, we cannot apply our method directly to these nanorods. Nevertheless, the theory can be used to explain the behavior of wider particles with the same aspect ratio (10 : 1) of the nanorods. In doing so, the physical parameters of our analysis are summarized in Table II. Finally, our choice of the levitation plane position at $z_{\text{eq}} = 0.85H/2$ is arbitrary, but compatible with the previous reported levitation height of Au particles⁵⁵, $0.41H/2 < z_{\text{eq}} < H/2$. Hence, according to Eq. (34), the corresponding energy density for the chosen height of the levitation plane is $E_0 = 15.3 \text{ J m}^{-3}$.

With all model parameters in place, we can compute some features of the microspheroid behavior at the nodal plane for the (011) and (021) acoustic modes. The results are summarized in Table III. The characteristic trap time is of the order of seconds, and the reorientation time is about 31 ms. Besides, the microspheroid can be as fast as one body length per second. Note also the rigid walled chamber yields the largest radiation forces. In contrast, the radiation torque does not change with the chamber boundary conditions at all.

In Fig. 2, we show the radiation force field (red arrows) acting on the microspheroid aligned with the x axis as a function of the scaled coordinates x/R and y/R . The background contour plot corresponds to the force potential U_{011} , which appears radially symmetric at $z_{\text{eq}} = 0.85H/2$. Panels (a) and (b) display the results for soft and hard lateral boundary conditions, respectively. The bluish region corresponds to the middle trap, while the dotted-purple circle at $\varrho/R = 1$ in panel (b) illustrates the annular trap.

In Fig. 3, we show the radiation torque field (red arrows) on the microspheroid as a function of the scaled Cartesian coordinates. Both soft and hard wall chambers are considered with the (011) acoustic mode. The background contour plot is the radiation torque amplitude normalized to the characteristic torque $\tau_0 = 48.07 \text{ pN } \mu\text{m}$. The microspheroid position is at $(\varrho, \varphi, 0.85H/2)$, with orientation along the radial direction $\alpha = \varphi$ and $\beta = \pi/4$. We note the radiation torque has radial symmetry and points to the tangential direction \mathbf{e}_φ —see the inset in panel (b). Also, a larger radiation torque is achieved in the middle area with nearly the same amplitude in both chambers. Though the soft chamber develops a more homogeneous torque around the central area of the levitation plane. The principal effect of the radiation torque is to reorient the particle to the angular position $\beta = \pi/2$. In Table III, we see the reorientation characteristic time

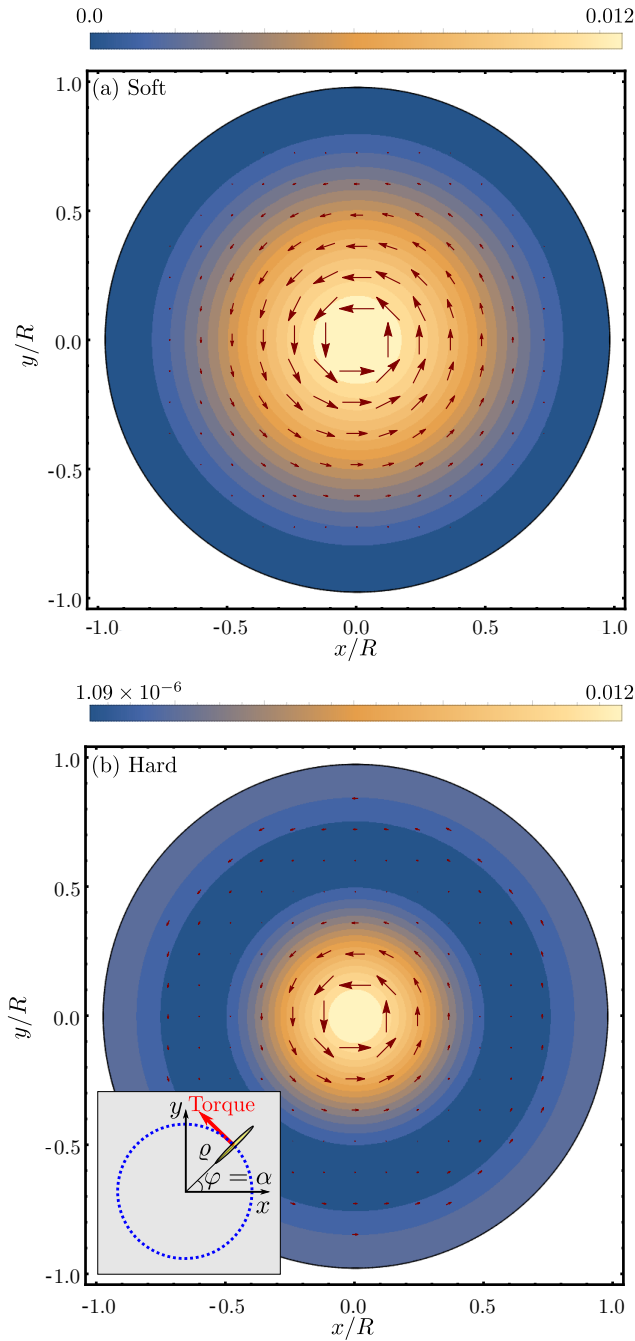


FIG. 3. The radiation torque fields (red arrows) in the levitation plane at $z_{\text{eq}} = 0.85H/2$ produced by the (011) acoustic mode for (a) a soft and (b) hard lateral wall. The background contours illustrate the radiation torque amplitude from Eq. (32) and normalized to $\tau_0 = 23.9 \text{ nN}\mu\text{m}$. The inset of panel (b) shows the microspheroid (in yellow) at the position (ϱ, φ) , aligned with the radial direction ($\alpha = \varphi$), and with $\beta = \pi/4$. The radiation torque is always perpendicular to the particle orientation. The physical parameters used here are listed in Table II.

is about $t_\beta = 30 \text{ ms}$. Moreover, it is independent of the lateral boundary conditions.

The particle reorientation effect was observed in millimeter-sized paper fibers caused by a standing plane wave at 72 kHz in water.²² A similar conclusion was achieved for polystyrene fibers with one-fourth of the wavelength in an acoustic resonator filled with water.²³ Nonetheless, an intriguing experimental observation in microgravity shows that a cluster of trapped 3 μm -long nanorods in water are aligned perpendicularly to the nodal plane inside a cylindrical chamber.⁵⁶ On this matter, we offer the following explanation for this effect. Firstly, the fluid viscosity may play a significant role in the radiation torque changing the orientation equilibrium position. Secondly, with the inter-particle distances being about the particle dimensions, the secondary radiation force becomes dominant.^{57,58} So one may expect the rise of secondary radiation torques. In turn, the secondary interaction torques are likely to change the particle orientation equilibrium. Thirdly, both density and geometric asymmetries seem to have a markedly influence on the nanorods behavior.²⁸ None of these features are taken into account by our approach.

V. CONCLUDING REMARKS

In this study, we present analytical results of the acoustic radiation force and torque developed on a rigid (prolate) spheroidal particle inside an ideal cylindrical chamber. The particle is considered far smaller than the acoustic wavelength and much larger than viscous boundary layers. The ideal chamber comprises a rigid bottom and top, with hard or soft lateral walls. The radiation force and torque expressions are given in the laboratory frame, paving the way to investigating the particle behavior through equations of motion. This approach can also be used for an incident wave of arbitrary shape, as long as the beam is expressed (analytically or numerically) in Cartesian or cylindrical coordinates.

The theory is applied to calculate the radiation forces and torques acting on a microspheroid. The model parameters are chosen to mimic the experimental setup of nanorods propelled by ultrasound.²⁶ As the nonviscous approximation is assumed, we could not apply theory directly to the nanorods. Notwithstanding, we keep the same aspect ratio of the nanorods (10 : 1) but consider a microspheroid with a diameter of 2 μm which is larger than the boundary layer depth. We obtain the characteristic radiation force and torque, and the particle translational and angular velocities of the first acoustic modes of the chamber. Furthermore, the particles in the nodal plane are reoriented to the same direction of this plane by means of the radiation torque. The reorientation time is of the order of milliseconds. Whereas, the radial trap occurs after several seconds passed.

Our model also predicts translational speeds of up to one body lengths per second (BLs^{-1}). The speed increases with the particle length squared. Should we applied the theory to the nanorods of Ref. 26, the speed

would be at least ten times smaller. This hints that the radial radiation force does not significantly impact the nanorods' propulsion mechanism.

The present analysis is a solid step toward understanding the physics behind trapping elongated particles in acoustofluidic settings. It offers results that can be verified experimentally for systems whose boundary conditions can be approximated to ideal conditions (hard or soft walls). Adding thermoviscous properties of the surrounding fluid to the model is the next level to be attained in future publications.

ACKNOWLEDGMENTS

G. T. Silva thanks the Brazilian National Council for Scientific and Technological Development–CNPq (Grant number 308357/2019-1), and Chaire Total ESPCI-Paris (2019).

APPENDIX A:

Going back to the transformation in Eq. (4b), we see the relation between the fluid velocity in the particle and laboratory frame is expressed as

$$\mathbf{v}_p(\mathbf{0}) = \mathbf{R}^{-1}(\alpha, \beta) \mathbf{v}(\mathbf{r}_0). \quad (\text{A1})$$

Thus, we have in Cartesian coordinates,

$$v_{x_p} = v_x \cos \alpha \cos \beta + v_y \sin \alpha \cos \beta - v_z \sin \beta, \quad (\text{A2a})$$

$$v_{y_p} = v_y \cos \alpha - v_x \sin \alpha, \quad (\text{A2b})$$

$$v_{z_p} = v_x \cos \alpha \sin \beta + v_y \sin \alpha \sin \beta + v_z \cos \beta. \quad (\text{A2c})$$

The corresponding components in to cylindrical coordinates are obtained using $v_x = v_\varrho \cos \varphi$, $v_y = v_\varrho \sin \varphi$,

$$v_{x_p} = v_\varrho \cos \beta \cos(\alpha - \varphi) - v_z \sin \beta, \quad (\text{A3a})$$

$$v_{y_p} = -v_\varrho \sin(\alpha - \varphi), \quad (\text{A3b})$$

$$v_{z_p} = v_\varrho \cos(\alpha - \varphi) \sin \beta + v_z \cos \beta. \quad (\text{A3c})$$

¹A. Ozcelik, J. Rufo, F. Guo, Y. Gu, P. Li, J. Lata, and T. J. Huang, “Acoustic tweezers for the life sciences,” *Nat. Methods* **15**, 1021–1028 (2018).

²G. T. Silva, J. H. Lopes, J. P. L. ao Neto, M. K. Nichols, and B. W. Drinkwater, “Particle patterning by ultrasonic standing waves in a rectangular cavity,” *Phys. Rev. Applied* **11**, 054044 (2019).

³P. Mishra, M. Hill, and P. Glynne-Jones, “Deformation of red blood cells using acoustic radiation forces,” *Biomicrofluidics* **8**, 034109 (2014).

⁴G. T. Silva, L. Tian, A. Franklin, X. Wang, X. Han, S. Mann, and B. W. Drinkwater, “Acoustic deformation for the extraction of mechanical properties of lipid vesicle populations,” *Phys. Rev. E* **99**, 063002 (2019).

⁵G. R. Torr, “The acoustic radiation force,” *Am. J. Phys.* **52**, 402–408 (1984).

⁶M. A. S. Pessoa and A. A. R. Neves, “Acoustic scattering and forces on an arbitrarily sized fluid sphere by a general acoustic field,” *J. Sound Vib.* **479**, 115373 (2020).

⁷B. T. Hefner and P. L. Marston, “An acoustical helicoidal wave transducer with applications for the alignment of ultrasonic and underwater systems,” *J. Acoust. Soc. Am.* **106**, 3313 (1999).

⁸A. Anhäuser, R. Wunenburger, and E. Brasselet, “Acoustic rotational manipulation using orbital angular momentum transfer,” *Phys. Rev. Lett.* **109**, 034301 (2012).

⁹L. Zhang and P. L. Marston, “Angular momentum flux of non-paraxial acoustic vortex beams and torques on axisymmetric objects,” *Phys. Rev. E* **84**(6), 065601 (2011).

¹⁰G. T. Silva, T. P. Lobo, and F. G. Mitri, “Radiation torque produced by an arbitrary acoustic wave,” *Europhys. Lett.* **97**, 54003 (2012).

¹¹G. T. Silva, “Acoustic radiation force and torque on an absorbing compressible particle in an inviscid fluid,” *J. Acoust. Soc. Am.* **136**, 2405–2413 (2014).

¹²I. D. Toftul, K. Y. Bliokh, M. I. Petrov, and F. Nori, “Acoustic radiation force and torque on small particles as measures of the canonical momentum and spin densities,” *Phys. Rev. Lett.* **123**, 183901 (2019).

¹³M. Baudoin and J.-L. Thomas, “Acoustic tweezers for particle and fluid micromanipulation,” *Annu. Rev. Fluid Mech.* **52**, 205–234 (2019).

¹⁴M. Barmatz and P. Collas, “Acoustic radiation potential on a sphere in plane, cylindrical, and spherical standing wave fields,” *J. Acoust. Soc. Am.* **77**, 928–945 (1985).

¹⁵M. Gröschl, “Ultrasonic separation of suspended particles - Part I: Fundamentals,” *Acta Acust. United. Ac.* **84**, 432–447 (1998).

¹⁶G. Goddard and G. Kaduchak, “Ultrasonic particle concentration in a line-driven cylindrical tube,” *J. Acoust. Soc. Am.* **117**, 3440–3447 (2005).

¹⁷S. M. Hagsäter, T. G. Jensen, H. Bruus, and J. P. Kuttera, “Acoustic resonances in microfluidic chips: full-image micro-PIV experiments and numerical simulations,” *Lab Chip* **7**, 1336–1344 (2007).

¹⁸A. P. Zhuk, V. D. Kubenko, and Y. A. Zhuk, “Acoustic radiation force on a spherical particle in a fluid-filled cavity,” *J. Acoust. Soc. Am.* **132**, 2189–2197 (2012).

¹⁹J. P. Leão-Neto and G. T. Silva, “Acoustic radiation force and torque exerted on a small viscoelastic particle in an ideal fluid,” *Ultrasonics* **71**, 1–11 (2016).

²⁰J. H. Lopes, M. Azarpeyvand, and G. T. Silva, “Acoustic interaction forces and torques acting on suspended spheres in an ideal fluid,” *IEEE Trans. Ultrason. Ferroelectr. Freq. Control* **63**, 186–97 (2016).

²¹D. Xu, F. Cai, M. Chen, F. Li, C. Wang, L. Meng, D. Xu, W. Wang, J. Wu, and H. Zheng, “Acoustic manipulation of particles in a cylindrical cavity: Theoretical and experimental study on the effects of boundary conditions,” *Ultrasonics* **93**, 18–25 (2019).

²²P. Brodeur, “Motion of fluid-suspended fibres in a standing wave field,” *Ultrasonics* **29**, 302–307 (1990).

²³S. Yamahira, S.-I. Hanaka, M. Kuwabara, and S. Asai, “Orientation of fibers in liquid by ultrasonic standing waves,” *Jpn. J. Appl. Phys.* **39**, 3683 (2000).

²⁴M. Saito, T. Daian, K. Hayashi, and S.-Y. Izumida, “Fabrication of a polymer composite with periodic structure by the use of ultrasonic waves,” *J. Appl. Phys.* **83**, 3490–3494 (1998).

²⁵T. Schwarz, P. Hahn, G. Petit-Pierre, and J. Dual, “Rotation of fibers and other non-spherical particles by the acoustic radiation torque,” *Microfluid Nanofluid* **18**, 65 (2015).

²⁶W. Wang, L. A. Castro, M. Hoyos, and T. E. Mallouk, “Autonomous motion of metallic microrods propelled by ultrasound,” *ACS Nano* **67**, 6122–6132 (2012).

²⁷S. Ahmed, D. T. Gentekos, C. A. Fink, and T. E. Mallouk, “Self-assembly of nanorod motors into geometrically regular multimers and their propulsion by ultrasound,” *ACS Nano* **8**, 11054–11060 (2014).

- ²⁸D. Ahmed, A. Ozcelik, N. Bojanala, N. Nama, A. U. Y. Chen, W. Hanna-Rose, and T. J. Huang, “Rotational manipulation of single cells and organisms using acoustic waves,” *Nat. Comms.* **7**, 11085 (2016).
- ²⁹S. Gutierrez-Ramos, M. Hoyos, and J. Ruiz-Surez, “Induced clustering of *Escherichia coli* by acoustic fields,” *Sci. Rep.* **8**, 4668 (2018).
- ³⁰P. L. Marston, W. Wei, and D. B. Thiessen, “Acoustic radiation force on elliptical cylinders and spheroidal objects in low frequency standing waves,” in *AIP Conf. Proc.*, 838 (2006), pp. 495–499.
- ³¹G. T. Silva and B. W. Drinkwater, “Acoustic radiation force exerted on a small spheroidal rigid particle by a beam of arbitrary wavefront: Examples of traveling and standing plane waves,” *J. Acoustic. Soc. Am.* **144**, EL453 (2018).
- ³²Z. Fan, D. Mei, K. Yang, and Z. Chen, “Acoustic radiation torque on an irregularly shaped scatterer in an arbitrary sound field,” *J. Acoust. Soc. Am.* **124**, 2727–2732 (2008).
- ³³J. P. Leo-Neto, J. H. Lopes, and G. T. Silva, “Acoustic radiation torque exerted on a subwavelength spheroidal particle by a traveling and standing plane wave,” *J. Acoust. Soc. Am.* **147**, 2177–2183 (2020).
- ³⁴T. S. Jerome and M. F. Hamilton, “Acoustic radiation force and torque on inhomogeneous particles in the born approximation,” *Proc. Mtgs. Acoust.* **39**, 045007 (2019).
- ³⁵T. S. Jerome, Y. A. Ilinskiy, E. A. Zabolotskaya, and M. F. Hamilton, “Born approximation of acoustic radiation force and torque on soft objects of arbitrary shape,” *J. Acoust. Soc. Am.* **145**, 36 (2019).
- ³⁶J. H. Lopes, E. B. Lima, J. P. Leão-Neto, and G. T. Silva, “Acoustic spin transfer to a subwavelength spheroidal particle,” *Phys. Rev. E* **101**, 043102 (2020).
- ³⁷P. Glynne-Jones, P. P. Mishra, R. J. Boltryk, and M. Hill, “Efficient finite element modeling of radiation forces on elastic particles of arbitrary size and geometry,” *J. Acoust. Soc. Am.* **133**, 1885 (2013).
- ³⁸P. Hahn, I. Leibacher, T. Baasch, and J. Dual, “Numerical simulation of acoustofluidic manipulation by radiation forces and acoustic streaming for complex particles,” *Lab. Chip.* **15**, 4302–4313 (2015).
- ³⁹F. B. Wijaya and K.-M. Lim, “Numerical calculation of acoustic radiation force and torque acting on rigid non-spherical particles,” *Acta Acust. united Ac.* **101**, 531 (2015).
- ⁴⁰Z. Gong, P. L. Marston, and W. Li, “*T*-matrix evaluation of three-dimensional acoustic radiation forces on nonspherical objects in Bessel beams with arbitrary order and location,” *Phys. Rev. E* **99**, 063004 (2019).
- ⁴¹Z. Gong, P. L. Marston, and W. Li, “Reversals of Acoustic Radiation Torque in Bessel Beams Using Theoretical and Numerical Implementations in Three Dimensions,” *Phys. Rev. Applied* **11**, 064022 (2019).
- ⁴²E. B. Lima, J. P. Leão Neto, A. S. Marques, G. C. Silva, J. H. Lopes, and G. T. Silva, “Nonlinear interaction of acoustic waves with a spheroidal particle: Radiation force and torque effects,” *Phys. Rev. Applied* **13**, 064048 (2020).
- ⁴³A. Tait, P. Glynne-Jones, A. Hill, D. E. Smart, C. Blume, B. Hammarstrom, A. L. Fisher, M. C. Gossel, E. J. Swindle, M. Hill, and D. E. Davies, “Engineering multi-layered tissue constructs using acoustic levitation,” *Sci. Rep.* **9**, 9789 (2019).
- ⁴⁴V. Garcia-Gradilla, S. Sattayasamitsathit, F. Soto, F. Kuralay, C. Yardmc, D. Wiitala, M. Galarnyk, and J. Wang, “Ultrasound-propelled nanoporous gold wire for efficient drug loading and release,” *Small* **10**, 4154–4159 (2014).
- ⁴⁵W. Wang, S. Li, L. Mair, S. Ahmed, T. J. Huang, and T. E. Mallouk, “Acoustic propulsion of nanorod motors inside living cells,” *Angew. Chem.* **126**, 3265–3268 (2014).
- ⁴⁶F. Nadal and E. Lauga, “Asymmetric steady streaming as a mechanism for acoustic propulsion of rigid bodies,” *Phys. Fluids* **26**, 082001 (2014).
- ⁴⁷J. F. Collis, D. Chakraborty, and J. E. Sader, “Autonomous propulsion of nanorods trapped in an acoustic field,” *J. Fluid Mech.* **825**, 29–48 (2017).
- ⁴⁸K. Lippera, O. Dauchot, S. Michelin, and M. Benzaquen, “No net motion for oscillating near-spheres at low Reynolds numbers,” *J. Fluid Mech.* **866**, R1 (2019).
- ⁴⁹E. W. Weisstein, *Bessel Function Zeros. From MathWorld—A Wolfram Web Resource.* (accessed August 23, 2020), <https://mathworld.wolfram.com/BesselFunctionZeros.html>.
- ⁵⁰A. A. Doinikov, “Acoustic radiation pressure on a rigid sphere in a viscous fluid,” *Proc. Royal Soc. London A* **447**, 447–466 (1994).
- ⁵¹M. Settnes and H. Bruus, “Forces acting on a small particle in an acoustical field in a viscous fluid,” *Phys. Rev. E* **85**, 016327 (2012).
- ⁵²T. Baasch, A. Pavlic, and J. Dual, “Acoustic radiation force acting on a heavy particle in a standing wave can be dominated by the acoustic microstreaming,” *Phys. Rev. E* **100**, 061102 (2019).
- ⁵³C. P. Lee and T. G. Wang, “Near-boundary streaming around a small sphere due to two orthogonal standing waves,” *J. Acoust. Soc. Am.* **85**, 1081–1088 (1989).
- ⁵⁴S. Deo, “Stokes flow past a fluid prolate spheroid,” *Indian J. Pure Appl. Math.* **34**, 755–764 (2003).
- ⁵⁵G. Dumy, “Nanorods self-propulsion and optic ejection of particles in acoustic levitation,” Ph.D. thesis, Université de Paris, 2019.
- ⁵⁶G. Dumy, N. Jeger-Madiot, X. Benoit-Gonin, T. E. Mallouk, M. Hoyos, and J.-L. Aider, “Acoustic manipulation of dense nanorods in microgravity,” *Microgravity Sci. Tec.* (2020, in press).
- ⁵⁷G. T. Silva and H. Bruus, “Acoustic interaction forces between small particles in an ideal fluid,” *Phys. Rev. E* **90**, 063007 (2014).
- ⁵⁸S. Sepehrirahnama, K.-M. Lim, and F. S. Chau, “Numerical study of interparticle radiation force acting on rigid spheres in a standing wave,” *J. Acoust. Soc. Am.* **137**, 2614–2622 (2015).